

\$OPD 0DWHU 6WXGLRUXP 8QLYHUVLWç G  
\$UFKLYLR LVWLWX]LRQDOH GHOOD U

*modellin of the synthesis of o er nano arti les by means of a transferred ar t in tor h lasm  
system*

7KLV LV WKH ILQDO SHHU UHYLHZHG DXWKRUüV DFFHSWHG PDQXVFULSW S

*Published Version:*

%RVHOOL 0 \*KHUDUGL 0 &RORPER 9 ' PRGHOOLQJ RI WKH V\QV  
PHDQV RI D '& WUDQVIHUHG DUF WZLQ WRUFK SODVPD V\VWHP -2851\$/ 2  
> DE @

*Availability:*

This version is available at: <https://hdl.handle.net/11585/727909> since: 2020-02-17

*Published:*

DOI: <http://doi.org/10.1088/1361-6463/ab3607>

*Terms of use:*

*ome ri hts reserved The terms and onditions for the reuse of this version of the manus ri t are  
s e ified in the ublishin oli y or all terms of use and more information see the ublisher s ebsite*

7KLV LWHP ZDV GRZQORDGHG IURP ,5,6 8QLYHUVLWç GL %RORJQD  
:KHQ FLWLQJ SOHDVH UHIHU WR WKH SXEOLVKHG YHUV

*Arti le be ins on ne t a e*

This is the final peer-reviewed accepted manuscript of:

Tampieri F, Giardina A, Bosi FJ, et al.

Removal of persistent organic pollutants from water using a newly developed atmospheric plasma reactor

in *Plasma processes and polymers* 2018, 15, pp. 57-60

The final published version is available online at:

<https://doi.org/10.1002/ppap.201700207>

Rights / License:

The terms and conditions for the reuse of this version of the manuscript are specified in the publishing policy. For all terms of use and more information see the publisher's website.

This item was downloaded from IRIS Università di Bologna (<https://cris.unibo.it/>)

**When citing, please refer to the published version.**

## **Removal of persistent organic pollutants from water using a newly developed atmospheric plasma reactor**

Francesco Tampieri, Agata Giardina, Franco Javier Bosi, Alice Pavanello, Ester Marotta,\* Barbara Zaniol, Gabriele Neretti, Cristina Paradisi

---

Dr. Francesco Tampieri, Agata Giardina, Alice Pavanello, Prof. Ester Marotta, Prof. Cristina Paradisi

Department of Chemical Sciences, University of Padova, Via Marzolo 1, 35131 Padova, Italy

E-mail: ester.marotta@unipd.it

Dr. Franco Javier Bosi

Department of Industrial Engineering, University of Padova, Via Marzolo 9, 35131 Padova, Italy

Dr. Barbara Zaniol

Consorzio RFX, corso Stati Uniti 4, 35127 Padova, Italy

Dr. Gabriele Neretti

Department of Electrical, Electronic and Information Engineering, University of Bologna, Viale del Risorgimento 2, 40136 Bologna, Italy

---

A new bench-top reactor employing a streamer discharge in air was developed and tested for potential use in an advanced oxidation stage in water treatment processes. The complex heterogeneous system and the ensuing chemical processes were characterized using an integrated approach to map the morphology of the plasma/gas/liquid interface, identify the plasma short-lived excited species, determine the oxidants in solution and monitor the organic pollutants degradation. Three model pollutants were used in these experiments, Rhodamine B, phenol and Metolachlor. The first two are common standards used to evaluate the performance of advanced oxidation processes. Metolachlor is a widely used herbicide listed among the most important recalcitrant emerging organic pollutants. Energy efficiency, kinetics and products of our tests show a good performance of the reactor. Specifically, mineralization appears feasible also in the case of metolachlor.

# 1 Introduction

The search for novel and efficient technologies for advanced oxidation processes (AOPs) is warranted by the growing number of identified emerging organic contaminants (EOCs) found in waters and the concern for their ascertained or potential risks for the environment, in particular for the biosphere.<sup>[1, 2]</sup> Non-thermalizing electric discharges have long been exploited to produce ozone *ex-situ*, which is then used, alone or in combination with other AOPs, in strong oxidation treatment steps to degrade recalcitrant organic pollutants.<sup>[3]</sup> More recent developments use electrical discharges to generate non-thermal plasma in air in near proximity, in contact or within the water to be treated.<sup>[4-6]</sup> This approach benefits from the action of reactive species, present in the discharge zone or in its afterglow, which are much shorter lived and stronger oxidant than ozone. Different types of discharges, electrode configurations and reactor designs have been developed and tested<sup>[7, 8]</sup> in search for optimal performance in terms of efficiency of removal of the primary pollutant/s and of its/their transformation products (TPs). The strategic role of an air plasma based AOP is thus viewed in the context of an integrated water treatment process, as the stage to achieve the degradation of recalcitrant organic pollutants not necessarily all the way to carbon dioxide but to more easily oxidizable TPs. We have recently reported on the efficient AOP of phenol induced by a streamer discharge in air to form a plasma in contact with the phenol solution.<sup>[9]</sup> The good results obtained with that first prototype encouraged us to further pursue this approach. Thus, we built a new reactor and electrode assembly with improved design and using only inert materials to avoid possible contamination due to oxidative degradation of reactor parts. This is a stringent requirement in fundamental studies so as to avoid interferences in the quantitative chemical analyses necessary to characterize the new AOP, and besides, it is also necessary in the perspective of large scale developments. In addition, we used two interchangeable solution vessels: Pyrex glass for chemical and electrical measurements and quartz to characterize the plasma by optical emission spectroscopy (OES). This paper reports a description of the reactor and a characterization of the discharge and

ensuing reactive species obtained by means of OES and by chemical methods. The reactor was then tested in the treatment of a few representative organic pollutants in water, rhodamine B, phenol and metolachlor. Rhodamine B ([9-(2-carboxyphenyl)-6-diethylamino-3-xanthenylidene]-diethylammonium chloride) is a dye, widely used in the textile, print, dye and food industry.<sup>[10-12]</sup> Harmful effects of dyes residual in wastewaters have been reported<sup>[13-15]</sup> so their removal, especially from industrial effluents, is very important for the environment. Since its oxidation is easily monitored by UV-Vis spectroscopy, it was used to optimize experimental conditions such as the air flow, the interelectrode gap and the thickness of the aqueous solution. Phenol was used because it is a widespread organic pollutant and, due to its well-known reactions (rate constants and products) with different reactive oxygen species, sort of a standard for testing and comparing AOPs.<sup>[16-24]</sup> Finally, we studied the degradation of metolachlor ((RS)-2-Chloro-N-(2-ethyl-6-methyl-phenyl)-N-(1-methoxypropan-2-yl)acetamide), an emerging organic contaminant,<sup>[25]</sup> also largely diffused in wastewaters.<sup>[26]</sup> but, at best of our knowledge, not yet studied with plasma systems.

## **2 Experimental section**

### **2.1 Materials**

Rhodamine B (95%), phenol (99%), 2-nitrophenol (98%), 4-nitrophenol (98%), coumarin-3-carboxylic acid (97%), 7-hydroxycoumarin carboxylic acid (98%), potassium indigotrisulfonate, titanium (IV) oxysulfate sulfuric acid solution (27-31%), metolachlor, formic acid (98%) and acetonitrile (99.9%) were purchased from Sigma Aldrich. Ultrapure grade water (milliQ water) was obtained by filtration of deionized water with a Millipore system. Pure air used in the experiment was a synthetic mixture (80% nitrogen and 20% oxygen) from Air Liquide with specified impurities of H<sub>2</sub>O (< 3 ppm) and of CnHm (< 0.5 ppm).

## 2.2 Experimental Apparatus

A schematic and a picture of the plasma reactor are reported in Figure 1. It is made of a Pyrex cylindrical vessel (ID = 4.1 cm, OD = 4.5 cm, h = 6 cm, volume 80 mL ca.) closed by a Teflon cover. A stainless steel tube (ID = 4.0 mm, OD = 6.0 mm), inserted in the reactor along its axis through the top cover, serves as active electrode and as gas input channel. The end part of the tube is flared, reaching an inner diameter of 0.5 mm at its tip, thus injecting gas with higher velocity. The gas outlet port is also placed in the Teflon cover.

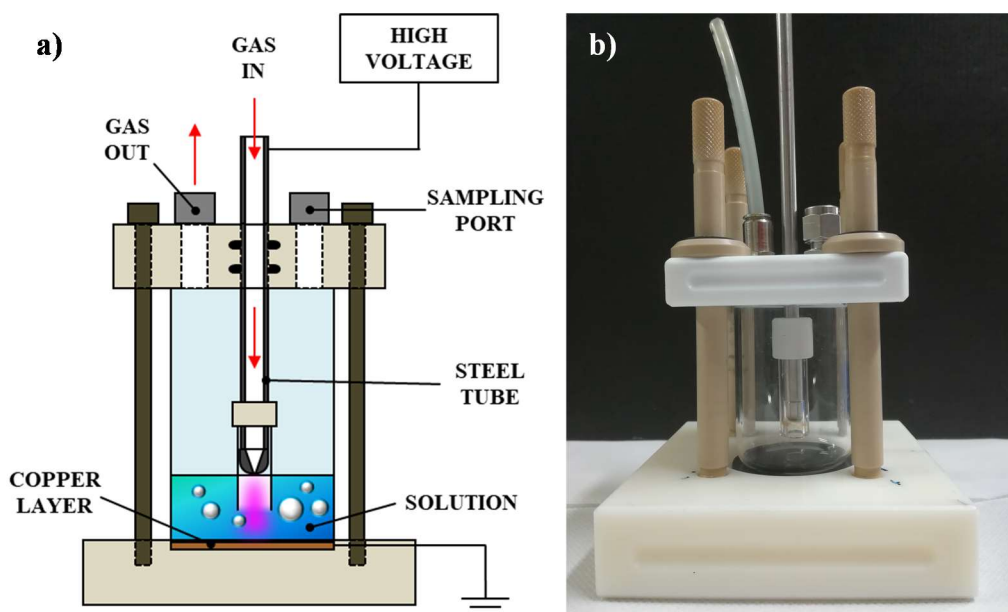


Figure 1. Reactor schematics (a) and picture (b).

The tip of the electrode touches the surface of the solution to be treated. The electrode lower part is embedded inside a Pyrex tube partially submerged in the solution (about 6 mm) with the purpose of forcing the gas to bubble within the liquid. As the gas flows in, an air pocket develops between the electrode tip and the liquid, which allows for the ignition of the discharge. The plasma is pushed against the liquid and penetrates it for 1-2 mm. The counter electrode is a thin copper layer in contact with the external surface of the vessel bottom and connected to the ground.

The whole set-up is gas-tight by means of Viton O-rings. The gas exiting from the reactor can be flowed through the cell of a FTIR spectrometer for gas analysis. In the top of the reactor there is also a sampling port, closed by a Teflon lined septum, used to withdraw solution samples with a syringe without removing the cover. For the OES measurements (see later), the Pyrex vessel and tube were substituted with others with same shape and dimension, but made of quartz. All the materials used to build the reactor (Pyrex, quartz, Teflon, Viton, stainless steel) were selected because they are not attacked by ozone that is formed when the discharge is on.

The electrical excitation is provided by a high voltage electronic transformer (maximum peak voltage 16 kV) that produces a modulated output into the 12-18 kHz frequency range.

The average power consumption was determined by means of voltage-current measurements. The high voltage probe was a Tektronix P6015A (75 MHz bandwidth), whereas the current probe was based on a shunt compression circuit designed as indicated in the literature.<sup>[27]</sup> The voltage-current signal was recorded by a Tektronix-TDS5032B digital phosphor oscilloscope set at 2 MHz sampling frequency.

During the experiments, a flow of air of 100 mL/min entered the reactor through the high voltage electrode and was bubbled into the solution. To minimize evaporation from the solution, the air was saturated with humidity by passing it through a water bubbler placed before the reactor. The volume of liquid used in the plasma treatment experiments was 15 mL.

### **2.3 Schlieren Imaging**

Schlieren images were obtained by a Z-type configuration setup.<sup>[28]</sup> A tungsten halogen low voltage lamp equipped with a rear reflector was used as light source. The condenser of the optical system was a Schneider-Kreuznach Xenon 40 mm double-Gauss lens with a f/1.9 focal ratio. Two off-axis parabolic mirrors of a diameter of 138 mm and an f/3.5 focal ratio reflected the light beam. Images were detected by a PCO CCD camera, equipped with a super-video-graphics array (SVGA)

resolution with a pixel size of  $6 \times 6 \mu\text{m}^2$ . The peak quantum efficiency was 55 % at a wavelength of 380 nm.

## **2.4 Emission Spectroscopy**

The spectroscopic system consisted of a PI-Acton spectrometer of 500 mm focal length equipped with a 1800 gr/mm grating and coupled to a PI-Pixis camera of 1340x400 square pixels of 13  $\mu\text{m}$ . With the entrance slit set at 50  $\mu\text{m}$ , the system had a resolution of about 50 pm at 500 nm. An optical head consisting of a fused silica lens of 50 mm focal length and 25 mm diameter focused the plasma light on a 1 mm core optical fibre. The fibre, also made of fused silica, was 5 m long and had the other end attached to the spectrometer entrance slit through an SMA connector. The spectral response of the system was measured from 350 nm to 700 nm using an integrating sphere. Only a relative intensity calibration was possible, since the small dimensions of the plasma did not fill the entrance f-number. The instrument function was measured with a Cd lamp, and resulted fully Gaussian with a full width at half maximum (fwhm) of 3.5 pixels. The lack of matching on f-numbers led to an effectively smaller fwhm. Its true value of 2.9 pixels, was found analyzing the rotational transitions of  $\text{N}_2$  spectra. The optical head was placed in front of the plasma source exit, looking directly on it. The weak plasma emission needed integration times ranging from 20 to 40 s.

## **2.5 Determination of Species produced by Plasma in Solution**

The pH of the solutions, after plasma treatment, was measured using a Mettler-Toledo S220 pH-meter equipped with an InLab Versatile Pro electrode.

The concentration of nitrate ions was measured by ion chromatography using a Dionex-ICS-900 instrument equipped with a Dionex IonPac AS22 IC Column after proper calibration with standard solution of  $\text{NaNO}_3$ . 4.5 mM sodium carbonate ( $\text{Na}_2\text{CO}_3$ ) and 1.4 mM sodium bicarbonate ( $\text{NaHCO}_3$ ) were used as the effluent at a flow rate of 1.2 mL/min for 15 min.

The concentration of ozone and hydrogen peroxide in solution were determined by the indigo<sup>[29]</sup> and titanium (IV) sulfate<sup>[30]</sup> methods, respectively. The rate of formation of hydroxyl radical was determined using coumarin-3-carboxylic acid as fluorescent probe.<sup>[31]</sup> All the procedures are described in detail in [9, 32].

## **2.6 Treatment of Organic Pollutants**

Solutions of the organic pollutant (rhodamine B, phenol, metolachlor) were prepared in milliQ water. We treated aliquots of 15 mL of solution for different times with a gas flow rate of 100 mL/min. Each point in the figures that have been reported in the Results and Discussion session corresponds to a single experiment. All the experiments were repeated at least twice, in order to verify the reproducibility.

The solutions of rhodamine B were analyzed with a Varian Cary 50 UV-Vis spectrophotometer running WinUV software. Absorbance data at 554 nm were collected and used to monitor the dye degradation profile.

The solutions of phenol were analyzed by HPLC/UV-Vis analysis (Shimadzu LC10AD pump with Shimadzu SPD-10A UV-Vis detector). An Agilent Zorbax Sb-Aq column (4.6 x 150 mm 3.5-Micron) was used with an eluent composed of 80% aqueous phosphate buffer (20 mM, pH = 2) and 20% acetonitrile. The elution was followed at 270 nm. The same analyses also allowed for the identification and determination of nitrophenols, which can form as undesired byproducts in air plasma treatment of phenol.<sup>[9, 33]</sup>

The solutions of metolachlor were analyzed by HPLC (Thermo Scientific Products instrument with P2000 pump and UV6000LP Diode array detector) at 270 nm. A Phenomenex Kinetex C18 column (5u C18 100A, 150x4.6 mm) was used and a mobile phase composed of water with 0.1% of formic acid (eluent A) and acetonitrile with 0.1% of formic acid (eluent B). The LC gradient for the

separation was: from 0 to 25 min, a linear increase of B from 5 to 95. The initial conditions were re-established in 5 min.

Standard solutions of rhodamine B, phenol, nitrophenols and metolachlor prepared at known concentrations were used for calibration.

The efficiency of degradation of the pollutants in the plasma treatment was evaluated using two parameters: the decay constant  $k$ , obtained by interpolation of experimental data using equation 1, and  $G_{50}^{[7]}$  (equation 2), the mass of pollutant converted divided by the energy required to reduce its quantity by one half,

$$C(t) = C_0 \cdot e^{-k \cdot t} \quad (1a)$$

$$C(E) = C_0 \cdot e^{-k \cdot E} \quad (1b)$$

$$G_{50}(g/kWh) = 1.8 \cdot 10^6 \frac{C_0(mol/L) \cdot V(L) \cdot MM(g/mol)}{P(W) \cdot t_{1/2}(s)} \quad (2)$$

where  $C_0$  and  $C$  are, respectively, the initial and residual pollutant concentration,  $t$  is the treatment time,  $E$  is the energy input,  $V$  is the volume of the treated solution,  $MM$  is the molar mass of the pollutant,  $P$  is the mean power of the reactor and  $t_{1/2}$  is the time required for the pollutant to achieve 50% conversion.

To measure the extent of mineralization achieved in the air plasma AOP, the solutions that were subjected to the longest treatment times were also analyzed for their total carbon content using a Shimadzu TOC -VCSN instrument, equipped with an autosampler and an automatic diluter. The instrument was calibrated using standard solutions of potassium hydrogen phthalate automatically diluted in the range of interest. Some constant carbon release was found and quantified in the reactor and was subtracted to the experimental measurements.

### 3 Results and discussion

#### 3.1 Characterization of the reactor

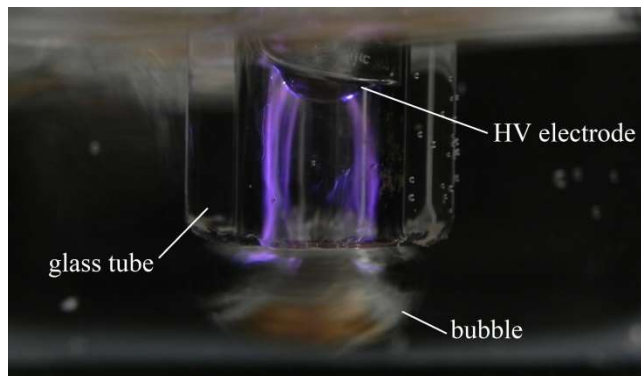


*Figure 2.* Photograph of the reactor during the generation of the discharge. Exposure time 125 ms.

Figure 2 reports a high resolution image of the reactor with the discharge on. The hemispheric tip of the HV electrode is seen inside the external protecting glass tube. An air bubble is coming out from the glass tube outlet immersed in the water. Several plasma streamers are clearly visible in the inner part of the tube. These filaments are produced on the HV electrode surface and then they propagate along the internal surface of the glass tube down to its edge. The approximate length of plasma streamers is about 6 mm.

We performed preliminary experiments using a solution of rhodamine  $1 \cdot 10^{-5}$  M in milliQ water in order to optimize the experimental conditions. Rhodamine B was chosen since its degradation can be easily monitored by means of UV-vis spectroscopy. The best conditions, i.e. those leading to the fastest degradation of the pollutant, were the following: solution volume 15 mL, gas flow rate 100 mL/min, distance between electrodes 13 mm. These conditions were then used in all experiments, unless otherwise stated. The data obtained in the degradation experiment with rhodamine B under these conditions are reported in Figure 3.

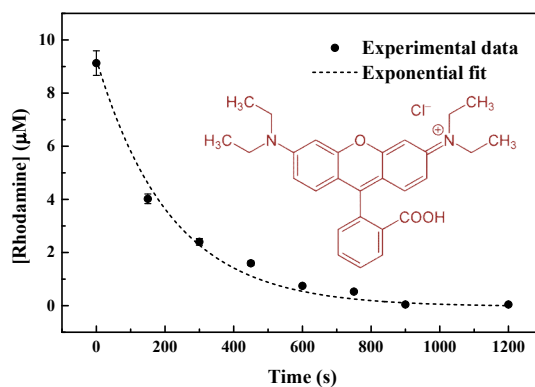


Figure 3. Rhodamine B conversion, as a function of treatment time in the plasma reactor. The black dashed lines are the best exponential fit of the experimental data to a first order exponential decay function.

Under these conditions complete decomposition of the starting pollutant was achieved within 15 min of treatment. By fitting the data in figure 3 with a first order exponential decay function we obtained the decay constant of rhodamine as  $k_t = (4.6 \pm 0.8) \cdot 10^{-3} \text{ s}^{-1}$ , that, by taking into account for the average power of the reactor (see later), can be express also in terms of energy  $k_E = (7.9 \pm 1.3) \cdot 10^{-4} \text{ J}^{-1}$ . The efficiency parameters relative to this experiment (half life time, decay constant and energy efficiency) are reported in Table 2 (see later).

An increase of the solution temperature has been measured, from room temperature up to 50 - 60 °C after 10 minutes of treatment. The measurements were performed after switching off the discharge and opening the reactor, so we expect the solution temperature to reach slightly higher values. This increase in the solution temperature could in principle affect the solubility of some species in solution and also the kinetics of some relevant processes.

Typical voltage and current profiles obtained with the reactor used are shown in Figure 4. The voltage signal is composed by the 50 Hz of the main grid modulated at high frequency (16 kHz) by the electric transformer. The average power of the reactor was estimated by integration of the voltage current signal. Average power was estimated by integration of the current voltage signal at different times during the tests. FFT analysis allowed us to estimate that the error caused by

sampling the signal at 2MHz is less than 1%, while that due to the shunt is less than 0.1%. The non uniform - transient nature of the streamer discharge is the only issue to be addressed in order to have an “average power” parameter to characterize the reactor. These fluctuations were observed to be within  $\pm 12\%$  of the average value determined for the power. No larger fluctuations in power were recorded, partly because the number of streamers produced is high enough, partly because the high voltage transformer is equipped with an internal ballast resistor that helps stabilize the discharge. Statistical averages of the different acquisitions showed that the reactor consumes about  $5.9 \pm 0.7$  W. Since, to a first approximation, the power can be assumed constant during our experiments, in the following sections, all results are given as a function of energy rather than as function of time. The energy was obtained by multiplying the treatment time by the average power.

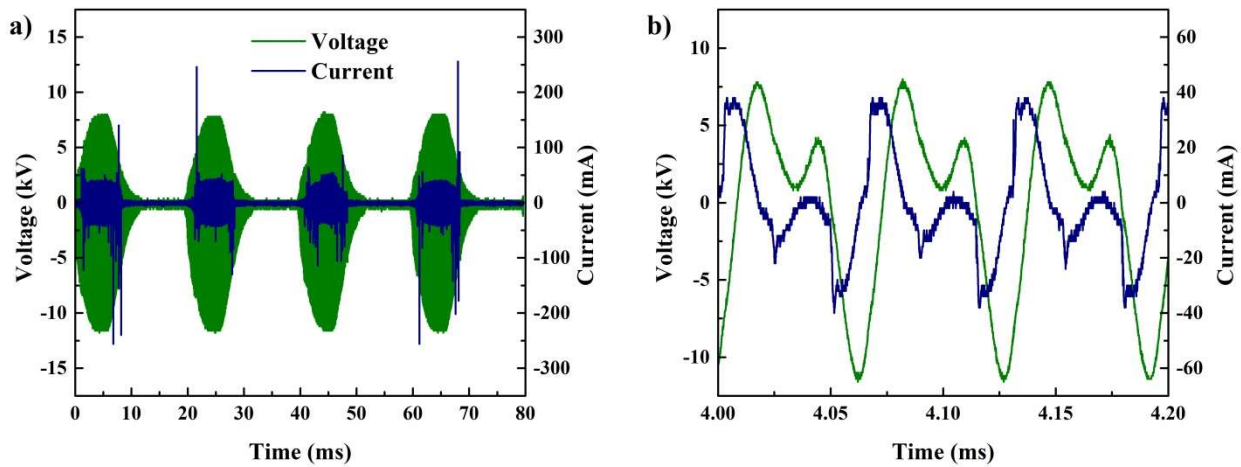


Figure 4. Voltage (—) and current (—) oscillograms with different timescales. a) modulation at 50 Hz; b) modulation at 16 kHz.

The influence of plasma generation on the air bubble structure/shape and consequently on the morphology of the air/water interface has been investigated by means of Schlieren imaging. This optical diagnostic is sensitive to refractive index gradients within a transparent medium. Figure 5 reports several images showing the evolution of a bubble without and with plasma. The exposure

time was set at 1 ms, with a frame rate of 22 Hz. For clarity, in Figure 5a a reference scale of 1 mm and the outlet portion of the glass tube are depicted. When the discharge is off, the air bubble first increases both in height and width (a, b, c), subsequently it enlarges in the horizontal direction (d), and finally it begins to ascend toward the water surface moving along the outer surface of the glass tube (e).

When the discharge is on, the bubble morphology drastically changes. In Figure 5f, a protrusion is clearly visible on the bubble surface. This protrusion is associated with the formation of a streamer within the glass tube, a phenomenon that is able to locally deposit a considerable amount of thermal energy in very short times (streamers typically last for tens of nanoseconds). This fast deposition of thermal energy leads to the generation of strong thermal gradients propagating from the inner part of the air bubble into the water, following the plasma streamer propagation path. Figure 5g shows the air bubble expanding against the hot water region previously warmed up by the plasma filament. In Figure 5h a new plasma streamer is produced. The hot water region still expands in the vertical direction after several tens of milliseconds (Figure 5i). When the bubble is moving up toward the water surface, the hot water region generated by the second streamer is still clearly visible (Figure 5l). New protrusions due to the formation of new streamers are also seen.

The presence of plasma strongly modifies the bubble morphology and consequently the interface between air and water. The presence of hot protrusions is consistent with the relatively high translational temperatures associated with plasma filaments (see later).

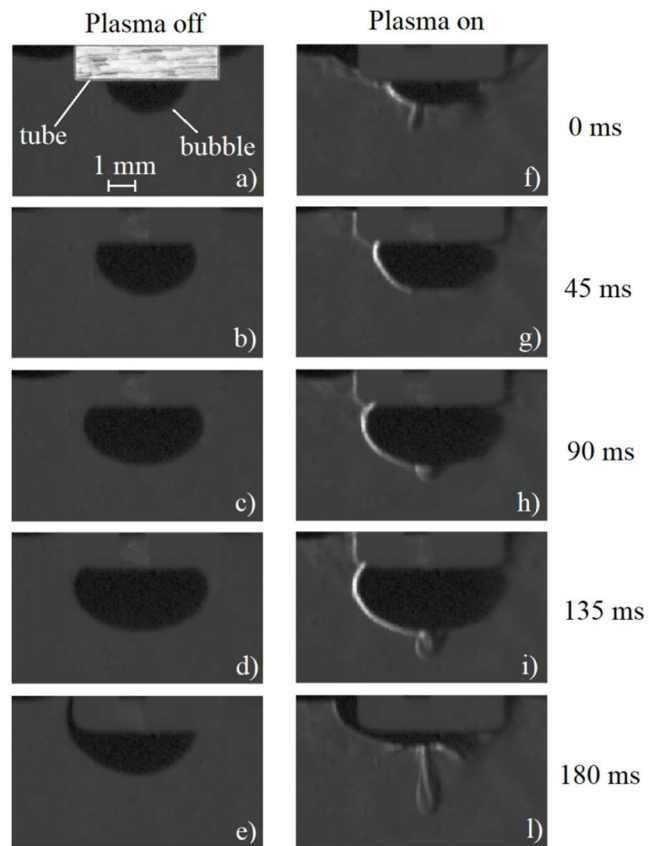


Figure 5. Time evolution of a bubble with the discharge off (a, b, c, d, e) and on (f, g, h, i, l).

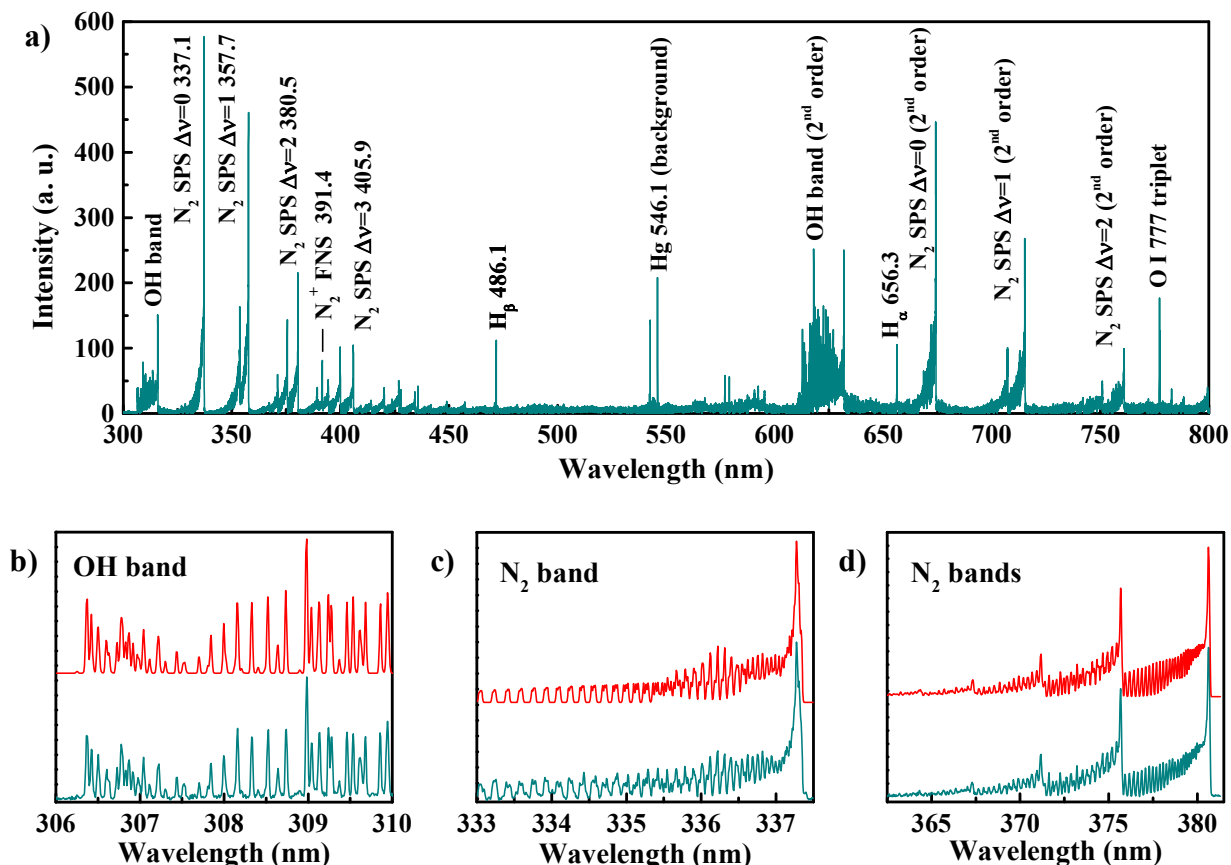


Figure 6. a) Typical raw spectrum acquired between 300 and 800 nm. The main emission lines have been identified. b) Second order OH band ( $A^2\Sigma, v = 0 \rightarrow X^2\Pi, v = 0$ ). c) Second order N<sub>2</sub> band ( $C^3\Pi_u, v = 0 \rightarrow B^3\Pi_g$ ) with  $\Delta v = 0$ . d) Second order N<sub>2</sub> band ( $C^3\Pi_u, v = 0 \rightarrow B^3\Pi_g$ ) with  $\Delta v = 2$ . The simulated spectra are also reported (red line).

The entire spectrum between 300 nm and 800 nm has been reconstructed by assembling together multiple acquisitions of different wavelength regions (see Figure 6a). The spectrum shows the N<sub>2</sub> ro-vibrational lines of the Second Positive System (SPS), the N<sub>2</sub><sup>+</sup> lines of the First Negative System (FNS), the OH band around 300 nm, then oxygen triplet at 777 nm, and the H<sub>α</sub> and H<sub>β</sub> lines. No filter was used to prevent the second diffraction order to overlap to the first one above 600 nm. In this way it was possible to collect OH and N<sub>2</sub> bands with a greater dispersion, which was most useful for determining the rotational temperatures of the two molecular species. The second order OH band at 306.357 nm ( $A^2\Sigma, v = 0 \rightarrow X^2\Pi, v = 0$ ) has been simulated for different rotational

temperatures.<sup>[34]</sup> By minimizing the integral of the squared differences between the simulations and the experimental spectrum a rotational temperature of  $2660 \pm 250$  K was derived (Figure 6b).

The same procedure was applied to the second order N<sub>2</sub> band at 337.1 nm ( $C^3\Pi_u, v = 0 \rightarrow B^3\Pi_g, v = 0$ ), using the atomic data reported in [35] for its simulation (Figure 6c). A rotational temperature of  $1700 \pm 150$  K was thus obtained. The rotational temperatures of the two molecular species are quite different. This difference has been observed already in literature for similar systems and in a 2014 review Bruggeman indicates the rotational temperature of N<sub>2</sub> as a better estimation of the gas temperature, with respect to that obtained from OH radicals that can be substantially overestimated.<sup>[36]</sup>

The vibrational temperature can be measured from the N<sub>2</sub> emissions corresponding to  $C^3\Pi_u \rightarrow B^3\Pi_g$  transitions with  $\Delta v = 2$ , under the hypothesis that the vibrational states population follows a Boltzmann distribution (Figure 6d). Assuming a rotational temperature of 1700 K, the 5 rotational bands between 360 and 380 nm were simulated and their relative intensities found by comparison with the experimental data. This procedure yielded a vibrational temperature, rescaled to the ground state, of about  $1500 \pm 200$  K, so compatible with the rotational temperature of the same molecules.

The electron temperature deduced by comparing the intensity ratio of first negative N<sub>2</sub><sup>+</sup> band at 391.4 nm and second positive N<sub>2</sub> band at 394.3 nm, in the hypothesis of being dominated by electron-impact excitation<sup>[37]</sup> was of  $1.7 \pm 0.5$  eV. Finally, the method reported in [38] was applied to the width of H <sub>$\alpha$</sub>  line, finding an electron density value of about  $6 \cdot 10^{20} \text{ m}^{-3}$ . Table 1 collects the main results obtained in plasma characterization by OES.

Table 1. Main parameters obtained by OES analysis of the plasma.

Parameter	Value
Electron density ( $\text{m}^{-3}$ )	$(6 \pm 2)10^{20}$
Ionization degree	$10^{-5}$
$T_e$ (eV)	$1.7 \pm 0.5$
$T_{\text{rot\_OH}}$ (K)	$2660 \pm 250$
$T_{\text{rot\_N}_2}$ (K)	$1700 \pm 150$
$T_{\text{vib}}$ (K)	$1500 \pm 200$

The performance of a plasma reactor in the degradation of persistent organic pollutants is mainly due to its efficiency in the production of reactive oxygen and nitrogen species. Figure 7 collects the results of chemical determinations of the species generated by plasma treatment in solution. First we observed a lowering of the pH of the solution by increasing the treatment time (Figure 7a) and a corresponding increase of the concentration of the nitrate ion (Figure 7b). The lowering of the pH is due to the formation of nitrogen oxides that by further reactions form nitric acid that dissociates in solution.<sup>[39]</sup> The concentrations of  $\text{NO}_3^-$  and  $\text{H}_3\text{O}^+$  are in agreement (about 2-4 mM after 30 min of treatment), meaning that the production of nitric acid is the main source of the pH decrease in our experimental setup.

We measured the concentration of ozone and hydrogen peroxide in the liquid phase (Figures 7c and 7d) using the procedure reported by Bader and Eisenberg respectively.<sup>[29, 30]</sup> Both species accumulate in water during the first part of the treatment, reach a maximum and are then consumed. These experimental data can be reproduced using a model typical of a transient species

$$C(E) = C_0 k_1 \frac{e^{-k_1 E} - e^{-k_2 E}}{k_2 - k_1} \quad (3)$$

where  $k_1$  and  $k_2$  are the formation and decomposition constant respectively, assuming simple unimolecular reactions. The maximum concentration of ozone in solution was about 14  $\mu\text{M}$ , after 300 s of treatment, corresponding to an energy input of 2 kJ. Hydrogen peroxide instead reached a maximum concentration of 0.5 mM after 800 s of treatment, corresponding to an energy of 4.5 kJ. The profiles of the two species are similar to those observed previously with a similar reactor.<sup>[9]</sup> Both species are produced and accumulate in solution during the first stages of treatment, then, other reactions, that consume them, prevail. Ozone is decomposed, in acidic solutions, by reacting with OH radicals and  $\text{NO}_2^-$ ;<sup>[40]</sup> similarly, also the reaction of hydrogen peroxide with  $\text{NO}_2^-$  ions is favorite under acidic conditions.<sup>[41]</sup>

The rate of formation of OH radicals in solution was measured following the procedure by Newton.<sup>[31]</sup> The assay uses coumarin-3-carboxylic acid (CCA), a chemical probe that reacts with OH radicals to give a fluorescent product 7-hydroxycoumarin carboxylic acid (7-CCA-OH). In Figure 7e the concentrations of 7-CCA-OH is reported as a function of the treatment energy. It grows linearly with energy in the first part of the graph and then reaches a plateau. This trend is due to two causes: CCA is decomposed significantly during plasma treatment, for the longest treatment times (Figure 7f), and correspondingly, 7-CCA-OH could become competitive in the reaction with OH radicals. By fitting linearly the first points, corresponding to a conversion of CCA of less than 20% (Figure 7f), it is possible to obtain the rate of formation of the hydroxylated product. With our reactor we obtained  $v_{7\text{-CCA-OH}} = (15.5 \pm 0.6) \mu\text{M kJ}^{-1}$ . Knowing that the yield of the reaction of formation of 7-CCA-OH is 4.7%<sup>[31]</sup> and assuming that 7-CCA-OH is not decomposed during the experiment (at least in the time/energy interval corresponding to the linear part of Figure 7e), we can calculate the rate of formation of OH radical. The hypothesis that the hydroxylated product is not significantly decomposed during the treatment is reasonable, since it is present in solution with a concentration at least 1000 times lower than that of its precursor (about  $10^{-3}$  M), so it cannot compete with it for the reaction with OH radicals. The value obtained for the rate of formation of

OH radical is  $v_{OH} = (330 \pm 13) \mu\text{M kJ}^{-1}$ , a value quite high if compared with other reactors designed for water treatment.<sup>[16]</sup>

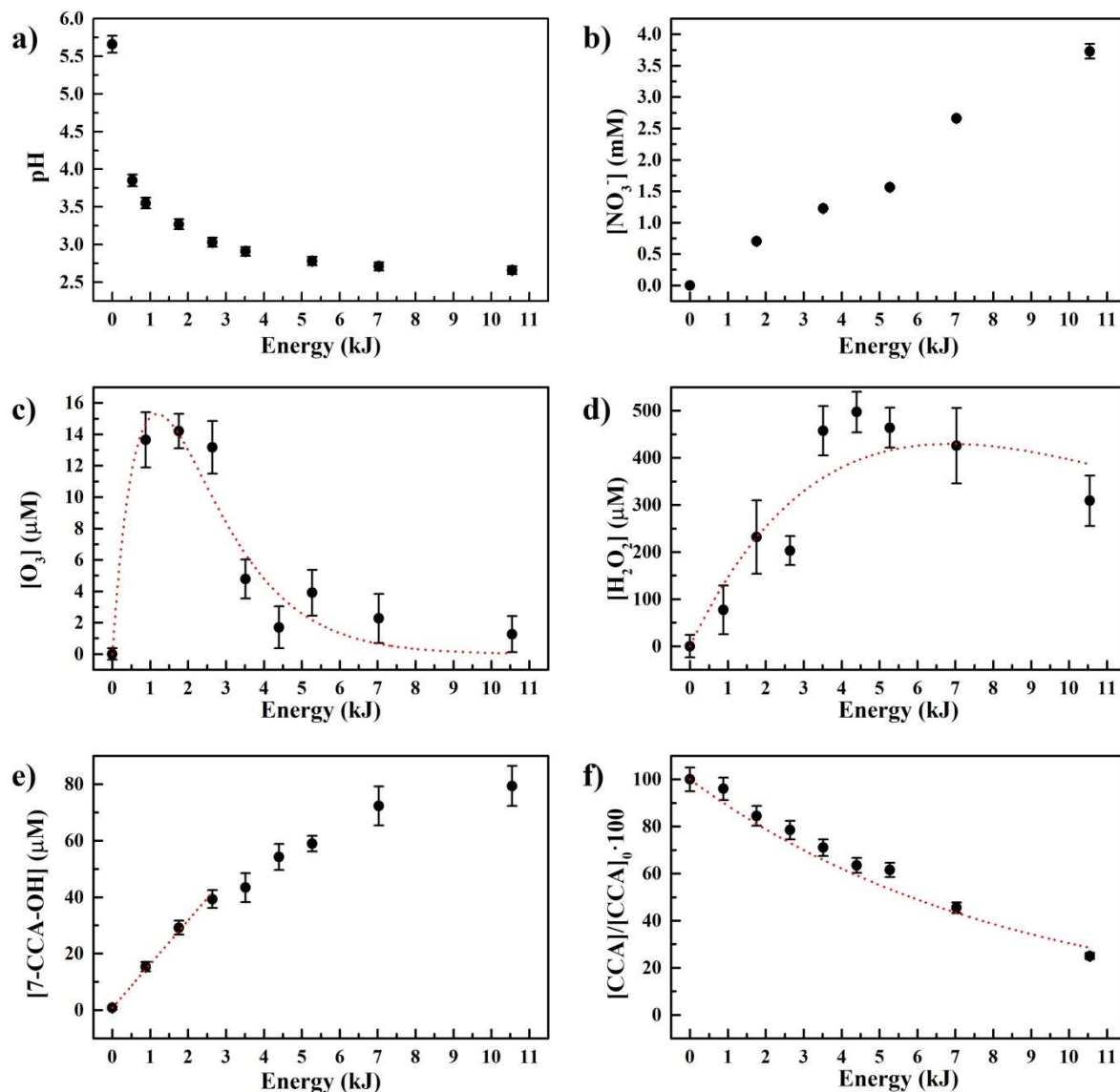


Figure 7. Species produced by plasma treatment as function of the energy of the process. a) pH; b) concentration of nitrate ions; c) concentration of ozone in solution; d) concentration of hydrogen peroxide; e) concentration of 7-CCA-OH; f) normalized concentration of CCA. The red dashed lines are the interpolations of the experimental data using eq. 3 (c and d), a straight line (e) and eq. 1b (f).

### 3.2 Removal of persistent organic pollutants

We tested the performance of our reactor by studying the oxidation of two representative persistent organic pollutants, phenol and metolachlor. Figure 8 summarizes the results of three experiments carried out with phenol at three different initial concentrations,  $1 \cdot 10^{-4}$ ,  $5 \cdot 10^{-4}$  and  $5 \cdot 10^{-5}$  M, respectively. The plots show the residual concentration of phenol as function of the energy. In the two more dilute solutions complete removal of phenol was achieved within 30 minutes of treatment; for the higher concentration, after 30 min, we observed less than 10% of phenol left in solution. By fitting the data with a first order exponential equation (eq. 1) we obtained the half life time and the decay constant relative to each experiment. We also computed the energy efficiency of the process (eq. 2). These data are collected in Table 2. It is seen, from Figure 8 and from the data in the table, that the decay constant depends on the initial concentration of the pollutant, the half-life time being 470, 230 and 170 s for initial concentrations of  $5 \cdot 10^{-4}$ ,  $1 \cdot 10^{-4}$  and  $5 \cdot 10^{-5}$  M, respectively. Our data are consistent with previous results reporting an inverse dependence of the decay constant in plasma treatment on the pollutants initial concentration <sup>[17]</sup>. On the other hand,  $G_{50}$ , the energy efficiency increases, by increasing the pollutant initial concentration. This behavior is also consistent with results reported and discussed earlier.<sup>[19, 21, 22, 42]</sup> The dependence of  $G_{50}$  on  $C_0$  is not easy to anticipate considering that also  $t_{1/2}$ , which appears in the denominator of eq. 2, depends on  $C_0$ .

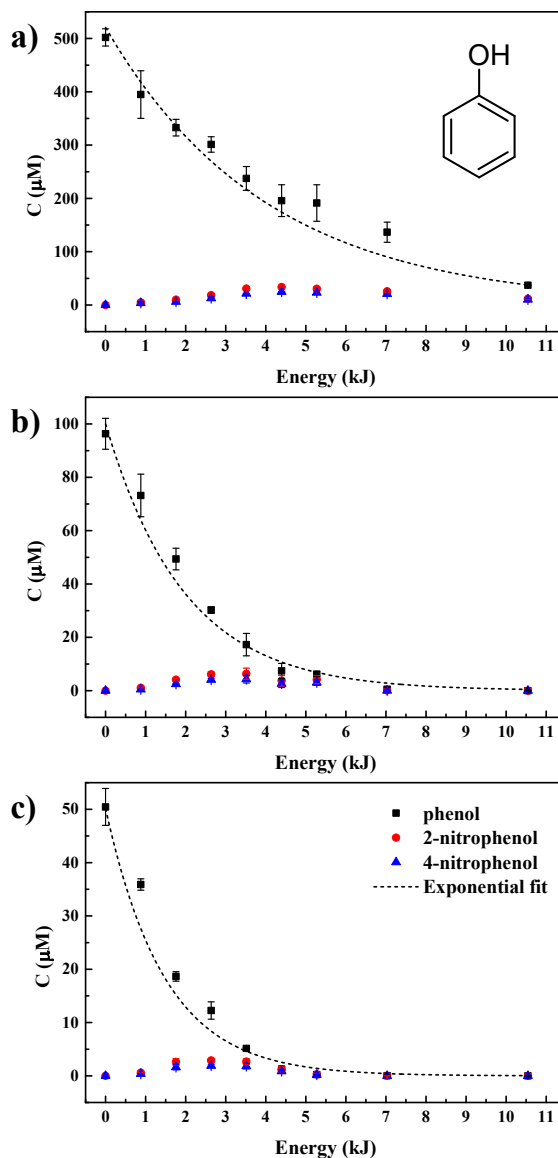


Figure 8. Concentration of phenol (■), 2-nitrophenol (●) and 4-nitrophenol (▲) as a function of energy in treatment of phenol in milliQ water with three initial concentrations: a)  $5 \cdot 10^{-4}$  M; b)  $1 \cdot 10^{-4}$  M; c)  $5 \cdot 10^{-5}$  M. The black dashed lines are the best fit of the experimental data to a first order exponential decay function.

It is known from the literature that plasma treatment of phenol in air generates 2- and 4-nitrophenol as byproducts due to side reactions of  $\text{NO}_x$ .<sup>[9, 33]</sup> Nitrophenols are more toxic and persistent than phenol itself,<sup>[33, 43, 44]</sup> so their formation is not desirable. We therefore searched for nitrophenols and monitored their formation and decay during the plasma treatment of phenol. Thus, for each experiment reported in Figure 8 we also show the concentration profiles of 2 and 4-nitrophenol. The

total amount of nitrophenols and their rate of formation and decay observed in our experiments depend on the initial concentration of phenol. Specifically, in experiments with phenol at  $C_0$  equal to  $5 \cdot 10^{-4}$ ,  $1 \cdot 10^{-4}$  and  $5 \cdot 10^{-5}$  M maximum nitrophenols concentrations of, globally, 60, 10 and 5  $\mu\text{M}$  were reached in 600, 450 and 300 s of treatment, respectively. Almost complete removal of nitrophenols from the solution was however achieved in all cases within the first 30 min of treatment.

The extent of mineralization achieved during the plasma treatment was also determined, by measuring the total organic carbon (TOC) in phenol solutions before treatment and after 30 minutes of treatment. The data are collected in Table 2. For the most concentrated solution ( $5 \cdot 10^{-4}$  M) a mineralization yield of  $(31 \pm 2)\%$  was obtained. For the less concentrated phenol solutions higher mineralization yields were achieved, notably  $(50 \pm 5)\%$  for the  $1 \cdot 10^{-4}$  M solution and  $(59 \pm 10)\%$  for the  $5 \cdot 10^{-5}$  M one. The high experimental errors associated with the mineralization yield of the more dilute solutions are due to sensitivity limits of the TOC analyzer.

*Table 2.* Half-life time ( $t_{1/2}$ ), decay constant ( $k_E$ ), energy efficiency ( $G_{50}$ ) and degree of mineralization achieved in 30 min plasma treatment of pollutants solutions in milliQ water.

<b>Pollutant</b>	<b><math>t_{1/2}</math> (s)</b>	<b><math>k_E</math> (<math>\text{J}^{-1}</math>)</b>	<b><math>G_{50}</math> (g <math>\text{kWh}^{-1}</math>)</b>	<b>%Mineralization</b>
Rhodamine B $1 \cdot 10^{-5}$ M	$150 \pm 20$	$(7.9 \pm 1.3) \cdot 10^{-4}$	$0.14 \pm 0.07$	n. d.
Phenol $5 \cdot 10^{-4}$ M	$471 \pm 9$	$(2.49 \pm 0.05) \cdot 10^{-4}$	$0.48 \pm 0.08$	$31 \pm 2$
Phenol $1 \cdot 10^{-4}$ M	$230 \pm 20$	$(5.2 \pm 0.4) \cdot 10^{-4}$	$0.19 \pm 0.06$	$50 \pm 5$
Phenol $5 \cdot 10^{-5}$ M	$170 \pm 10$	$(6.9 \pm 0.6) \cdot 10^{-4}$	$0.13 \pm 0.05$	$59 \pm 10$
Metolachlor $1 \cdot 10^{-4}$ M	$150 \pm 20$	$(7.7 \pm 1.2) \cdot 10^{-4}$	$0.9 \pm 0.3$	$20 \pm 3$

The results of plasma treatment of a solution of metolachlor with initial concentration  $1 \cdot 10^{-4}$  M are reported in Figure 9 and in Table 2. The rate of degradation of this pollutant is quite fast, with a

half-life time of about 150 s, resulting in complete removal from the solution within 20 minutes of treatment (Figure 9a). The energy efficiency of this experiment is quite high, especially if compared with those obtained with phenol and rhodamine in this work.

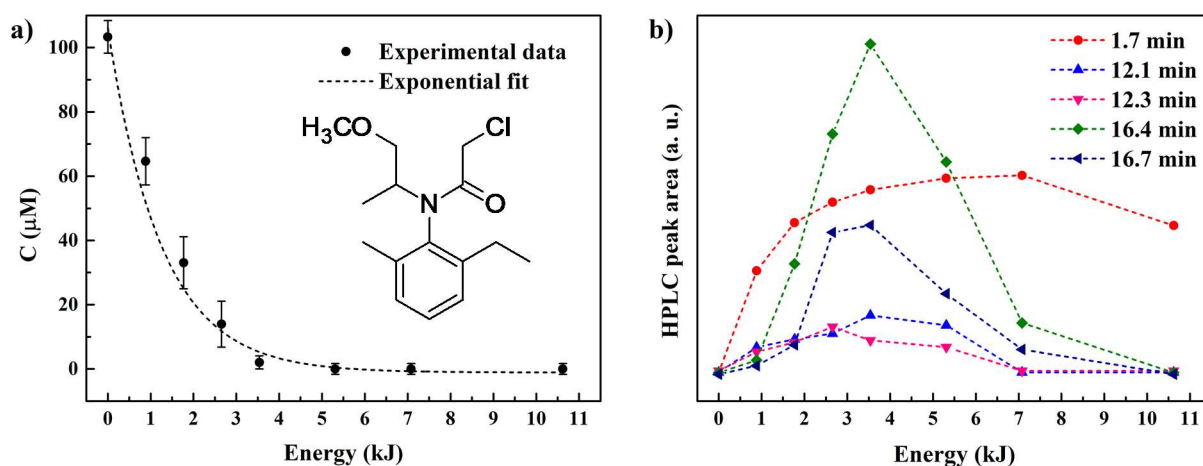


Figure 9. a) Decomposition of metolachlor (initial concentration:  $1 \cdot 10^{-4}$  M) in milliQ water. The black dashed line is the best exponential fit of the experimental data to a first order exponential decay function; b) evolution of metolachlor degradation products detected during the treatment. They are labelled according to their retention times. The dashed lines are just a guide for the eye.

From the HPLC-UV-Vis analysis at 270 nm of metolachlor treated samples we detected 5 oxidation products (Figure 9b), which show the typical profile of reaction intermediates, forming during the first part of the treatment, reaching a maximum and then decomposing at longer treatment times. It is interesting to note that all these intermediates except one were completely removed after 30 minutes of treatment. In the HPLC chromatograms we also observed other unresolved peaks at short retention times, reasonably attributed to small and highly oxidized organic compounds, notably carboxylic acids.

TOC analysis of the metolachlor solution treated in the plasma reactor for 30 min indicated a mineralization yield of 20%. This is a good result, considering the high initial concentration used ( $1 \cdot 10^{-4}$  M), the molecular complexity of metolachlor and the short treatment time. By increasing the

treatment time it is reasonable to expect higher oxidation degrees (as observed also by the analysis of the intermediates) and therefore higher mineralization extents.

## **4 Conclusions**

Building on previous screening of the performance of different discharge systems to bring about advanced oxidation of organic pollutants in water, we have developed a small prototype reactor based on a streamer discharge in air, which had tested as the most promising option in previous work. The reactor has features which make it suitable for fundamental kinetic and mechanistic studies on the advanced oxidation of emerging pollutants in water. It is built with inert materials to avoid contamination and interferences in the analysis of the advanced oxidation products and has a quartz vessel for optical emission spectroscopy characterization of the plasma. Thus, through a multidisciplinary approach and extensive complementary diagnostics the process was characterized in all of its major components: the plasma short-lived excited species and the ensuing reactive oxidizing species in solution, the morphology of the gas/plasma/liquid interface, the kinetics and efficiency of degradation of organic pollutants and the extent of mineralization achieved in their advanced oxidation.

Using phenol and Rhodamine B, common standards in the comparative evaluation of AOPs, the reactor performed quite satisfactorily with regard to the three major process parameters: duration and energy efficiency of the treatment and extent of mineralization achieved. It also tested positively in the treatment of metolachlor, a recalcitrant EOC (emerging organic contaminant), which was mineralized with a yield of 20% in 30 minutes. We found that in the present reactor the oxidation of metolachlor proceeds via several reaction steps and produces the same reaction intermediates observed when the treatment is carried out in the DBD reactor previously designed and fully investigated in our laboratory.<sup>[17]</sup> The product analysis and the reaction scheme are thus described in detail in a parallel study dealing with that reactor (submitted).<sup>[45]</sup>

**Acknowledgments.** We thank Stefano Mercanzin and Mauro Meneghetti for the construction of the reactor, University of Padova for financial support (grant CPDA147395/14 - Progetto di Ricerca di Ateneo 2014 and grants CPDR151800 and CPDR152275 - Progetti per Assegni di Ricerca Junior 2015) and COST Action TD1208 for the stimulating environment provided.

Received: ((will be filled in by the editorial staff)); Revised: ((will be filled in by the editorial staff)); Published online: ((will be filled in by the editorial staff))

**Keywords.** streamer discharge, metolachlor, phenol, reactive oxygen species, water treatment

## References

- [1] WWAP (United Nations World Water Assessment Programme), *The United Nations World Water Development Report 2017*.
- [2] L. P. Padhye, *Water Environ. Res.* **2016**, 88, 1619-1636.
- [3] C. Gottschalk, J. A. Libra, A. Saupe, *Ozonation of water and waste water: A practical guide to understanding ozone and its applications*, John Wiley & Sons, Weinheim, **2009**.
- [4] P. Bruggeman, M. Kushner, B. Locke, J. Gardeniers, W. Graham, D. Graves, R. Hofman-Caris, D. Maric, J. Reid, E. Ceriani, D. Fernandez Rivas, J. Foster, S. Garrick, Y. Gorbanev, S. Hamaguchi, F. Iza, H. Jablonowski, E. Klimova, J. Kolb, F. Krema, P. Lukes, Z. Machala, I. Marinov, D. Mariotti, S. Mededovic Thagard, D. Minakata, E. Neyts, J. Pawlat, Z. Lj Petrovic, R. Pflieger, S. Reuter, D. Schram, S. Schröter, M. Shiraiwa, B. Tarabová, P. Tsai, J. Verlet, T. von Woedtke, K. Wilson, K. Yasui, G. Zvereva, *Plasma Sources Sci. Technol.* **2016**, 25, 053002.
- [5] B. Jiang, J. Zheng, S. Qiu, M. Wu, Q. Zhang, Z. Yan, Q. Xue, *Chem. Eng. J.* **2014**, 236, 348-368.

- [6] P. Vanraes, A. Y. Nikiforov, C. Leys. *Electrical discharge as water treatment technology for micropollutant decomposition in Plasma Science and Technology - Progress in Physical States and Chemical Reactions* (Ed: Mieno Tetsu) Intech, 2016 DOI: 10.5772/60692.
- [7] M. A. Malik, *Plasma Chem. Plasma Process.* **2010**, *30*, 21-31.
- [8] G. R. Stratton, C. L. Bellona, F. Dai, T. M. Holsen, S. M. Thagard, *Chem. Eng. J.* **2015**, *273*, 543-550.
- [9] F. J. Bosi, F. Tampieri, E. Marotta, R. Bertani, D. Pavarin, C. Paradisi, *Plasma Process. Polym.*, **2017**, DOI: 10.1002/ppap.201700130.
- [10] A. Cassano, R. Molinari, M. Romano, E. Drioli, *J. Membr. Sci.* **2001**, *181*, 111-126.
- [11] D. Pokhrel, T. Viraraghavan, *Sci. Total Environ.* **2004**, *333*, 37-58.
- [12] O. Tünay, I. Kabdasli, G. Eremektar, D. Orhon, *Water Sci. Technol.* **1996**, *34*, 9-16.
- [13] R. D. Hood, C. L. Jones, S. Ranganathan, *Teratology* **1989**, *40*, 143-150.
- [14] T. W. Sweatman, R. Seshadri, M. Israel, *Cancer Chemother. Pharmacol.* **1990**, *27*, 205-210.
- [15] B. J. Y. Wuebbles, J. S. Felton, *Environ. Mutagen.* **1985**, *7*, 511-522.
- [16] E. Marotta, M. Schiorlin, X. Ren, M. Rea, C. Paradisi, *Plasma Process. Polym.* **2011**, *8*, 867-875.
- [17] E. Marotta, E. Ceriani, V. Shapoval, M. Schiorlin, C. Ceretta, M. Rea, C. Paradisi, *Eur. Phys. J. Appl. Phys.* **2011**, *55*, 13811.
- [18] E. Marotta, E. Ceriani, M. Schiorlin, C. Ceretta, C. Paradisi, *Water Res.* **2012**, *46*, 6239-6246.
- [19] E. Bobkova, E. Ivanova, R. Nevedomyi, A. Sungurova, *High Energy Chem.* **2014**, *48*, 346-349.
- [20] W. Hoebe, E. Van Veldhuizen, W. Rutgers, C. Cramers, G. Kroesen, *Plasma Sources Sci. Technol.* **2000**, *9*, 361.
- [21] N. Sano, T. Kawashima, J. Fujikawa, T. Fujimoto, T. Kitai, T. Kanki, A. Toyoda, *Ind. Eng. Chem. Res.* **2002**, *41*, 5906-5911.

- [22] N. Sano, Y. Yamane, Y. Hori, T. Akatsuka, H. Tamon, *Ind. Eng. Chem. Res.* **2011**, *50*, 9901-9909.
- [23] B. Sun, M. Sato, J. Clements, *Environ. Sci. Technol.* **2000**, *34*, 509-513.
- [24] L. Wang, X. Jiang, *J. Hazard. Mater.* **2009**, *161*, 926-932.
- [25] C. D. Tomlin, *The pesticide manual: a world compendium.*, British Crop Production Council **2009**.
- [26] M. Köck-Schulmeyer, M. Villagrasa, M. López de Alda, R. Céspedes-Sánchez, F. Ventura, D. Barceló, *Sci. Total Environ.* **2013**, *458-460*, 466-476.
- [27] D. Ashpis, M. Laun, E. Griebeler. *50th AIAA Aerospace Sciences Meeting Including the New Horizons Forum and Aerospace Exposition* **2012** 823.
- [28] G. Neretti, A. Cristofolini, C. A. Borghi, *J. Appl. Phys.* **2014**, *115*, 163304.
- [29] H. Bader, J. Hoigné, *Water. Res.* **1981**, *15*, 449-456.
- [30] G. Eisenberg, *Ind. Eng. Chem.* **1943**, *15*, 327-328.
- [31] G. L. Newton, J. R. Milligan, *Radiat. Phys. Chem.* **2006**, *75*, 473-478.
- [32] G. Neretti, F. Tampieri, C. A. Borghi, P. Brun, R. Cavazzana, L. Cordaro, C. Paradisi, E. Marotta, P. Seri, M. Taglioli, B. Zaniol, M. Zuin, E. Martines, submitted for publication.
- [33] E. Ceriani, E. Marotta, V. Shapoval, G. Favaro, C. Paradisi, submitted for publication.
- [34] C. De Izarra, *J. Phys. D* **2000**, *33*, 1697-1704.
- [35] G. Hartmann, P. C. Johnson, *J. Phys. B: At. Mol. B* **1978**, *11*, 1597-1612.
- [36] P. J. Bruggeman, N. Sadeghi, D. C. Schram, V. Linss, *Plasma Sources Sci. Technol.* **2014**, *23*, 023001.
- [37] N. Britun, M. Gaillard, A. Richard, Y. M. Kim, K. S. Kim, J. G. Han, *J. Phys. D: Appl. Phys.* **2007**, *40*, 1022.
- [38] N. Konjević, M. Ivković, N. Sakan, *Spectrochim. Acta, Part B*, **2012**, *76*, 16-26.
- [39] S. N. Pandis, J. H. Seinfeld, *J. Geophys. Res.* **1989**, *94*, 1105-1126.

- [40] R. Flyunt, A. Leitzke, G. Mark, E. Mvula, E. Reisz, R. Schick, C. von Sonntag, *J. Phys. Chem. B* **2003**, *107*, 7242-7253.
- [41] B. R. Locke, K. Shih, *Plasma Sources Sci. Technol.* **2011**, *20*, 034006.
- [42] P. M. K. Reddy, B. R. Raju, J. Karupiah, E. L. Reddy, C. Subrahmanyam, *Chem. Eng. J.* **2013**, *217*, 41-47.
- [43] J. Kiwi, C. Pulgarin, P. Peringer, *Appl. Catal. B Environ.* **1994**, *3*, 335-350.
- [44] J. Michałowicz, W. Duda, *Polish J. Environ. Stud.* **2007**, *16*, 347-362.
- [45] A. Giardina, E. Marotta, C. Paradisi, submitted for publication.

## Graphical Abstract

### Removal of persistent organic pollutants from water using a newly developed atmospheric plasma reactor

Francesco Tampieri, Agata Giardina, Franco Javier Bosi, Alice Pavanello, Ester Marotta,\* Barbara Zaniol, Gabriele Neretti, Cristina Paradisi

**A new reactor employing a streamer discharge in air was developed and tested for potential use in water treatment processes.** The system was characterized using an integrated approach to: map the morphology of the plasma/gas/liquid interface, identify the short-lived excited species, determine the oxidants in solution and monitor the organic pollutants degradation. Three model pollutants were used in these experiments, Rhodamine B, phenol and Metolachlor.

